Polymer 53 (2012) 4702–4708

Contents lists available at SciVerse ScienceDirect

Polymer

journal homepage: www.elsevier.com/locate/polymer

Orientation of poly(vinyl alcohol) nanofiber and crystallites in non-woven electrospun nanofiber mats under uniaxial stretching

Takahiro Yano [a], Yuji Higaki [a,b], Di Tao [a], Daiki Murakami [b], Motoyasu Kobayashi [b], Noboru Ohta [c], Jun-ichiro Koike [d], Misao Horigome [d], Hiroyasu Masunaga [c], Hiroki Ogawa [c], Yuka Ikemoto [c], Taro Moriwaki [c], Atsushi Takahara [a,b,*]

[a] Graduate School of Engineering, Kyushu University, Fukuoka, Japan
[b] Institute for Materials Chemistry and Engineering, Kyushu University, Fukuoka, Japan
[c] Japan Synchrotron Radiation Research Institute, SPring-8, Hyogo, Japan
[d] DIC Corporation, 631 Sakado, Sakura, Chiba 285-8688, Japan

ARTICLE INFO

Article history:
Received 1 April 2012
Received in revised form
21 July 2012
Accepted 31 July 2012
Available online 7 August 2012

Keywords:
Electrospinning
Poly(vinyl alcohol)
Orientation

ABSTRACT

The development of macroscopic nanofiber orientation and microscopic crystallite and molecular chain orientation have been investigated during uniaxial stretching of electrospun poly(vinyl alcohol) (PVA) non-woven nanofiber mats. Scanning electron microscopy and stress-strain/small-angle X-ray scattering show that the macroscopic nanofiber orientation significantly increases during the initial stage of deformation, and approaches a plateau on the way of stretching. Detailed analyses of the stress-strain/wide-angle X-ray diffraction measurement and polarized Fourier transform infrared spectroscopy indicate that the microscopic crystallite and molecular chain orientation rapidly increase at the initial stage of stretching due to macroscopic nanofiber orientation. At higher deformation, the microscopic modes of orientation continuously develop as a result of the nanofiber stretching. The complicated deformation process of non-woven nanofiber mats is discussed in terms of macroscopic nanofiber orientation and the microscopic crystallite and molecular chain orientation.

1. Introduction

Polymer nanofibers exhibit a number of unique properties, such as high mechanical strength and high glass transition temperature [1,2]. Non-woven fabrics composed of nanofibers are of particular interest due to their exceptionally high surface area to volume ratio. Non-woven nanofiber mats have potential applications for a number of fields, such as nanoparticle carriers, electronic sensors, filter membranes, and biodegradable scaffolds [3,4]. Electrospinning is a versatile technique for nanofiber fabrication [5–9], because the fiber diameter can be easily controlled from the nano- to sub-micron scale by manipulating fiber fabrication conditions and solvent [10–13]. The crystalline structure and crystalline orientation of electrospun semi-crystalline polymer nanofibers are significantly affected by fiber geometry and fabrication conditions [14–17], which will strongly influence physical properties. For example, Schaper et al. reported that the crystalline structure and molecular orientation of electrospun polyethylene (PE) nanofibers depend on fiber diameter [14]. The PE nanofibers exhibit a shish-kebab structure consisting of discotic lamellar kebabs that extend perpendicular from a high molecular weight interior shish structure. Larger diameter fibers show relatively weak orientation of the kebabs, whereas fibers with diameter below 400 nm form highly extended chain structures along the fiber axis, with much higher degree of crystalline orientation. Chirachanchai et al. have reported control of the crystal structure of electrospun poly(oxymethylene) (POM) nanofibers by manipulating the applied voltage and take-up velocity [15]. They experimentally demonstrated that the extended chain crystal component increases with take-up velocity, whereas the folded chain crystal component decreases. Most previous studies have focused on the crystalline structure of nanofibers induced by the fabrication process and the post-annealing process.

Various attempts have been undertaken to understand the mechanical properties of electrospun nanofiber mats [18,19]. Stress-strain behavior of the nanofiber mat strongly depends on the fiber geometry and processing conditions, and is generally attributed to crystalline and molecular chain orientation. However, electrospun nanofiber mats contain a large number of defects due to the random orientation of fibers and the presence of dangling

* Corresponding author. Institute for Materials Chemistry and Engineering, Kyushu University, 744 Motooka, Nishi-ku, Fukuoka 819-0395, Japan. Tel.: +81 928022517; fax: +81 928022518.
E-mail address: takahara@cstf.kyushu-u.ac.jp (A. Takahara).

0032-3861/$ – see front matter © 2012 Elsevier Ltd. All rights reserved.
http://dx.doi.org/10.1016/j.polymer.2012.07.067

fibers, which result in inhomogeneous stress distribution. Furthermore, the crystalline structure and molecular chain orientation are modified during mechanical deformation, and in the case of nanofiber mats, macroscopic fiber orientation will also take place. The development of both macroscopic and microscopic orientation will certainly contribute to the non-woven fiber mat mechanical properties. However, the presence of structural defects significantly complicates this process and has so far prevented detailed investigation of structural development of the non-woven nanofiber mats during mechanical deformation.

In-situ simultaneous stress-strain small-angle X-ray scattering (SAXS)/wide-angle X-ray diffraction (WAXD) measurement with synchrotron radiation is a powerful tool for the investigation of structural development of polymer materials. Combining the high intensity of a synchrotron radiation X-ray source with precision detectors enables a wide range of structural details to be studied on a single specimen during mechanical deformation. This technique has been previously applied to investigate structural development in polymer films [20–25]. The influence of crystalline orientation, orientation-induced crystallization, crystal transition, fibrillar formation and cavitation on the film deformation process has been demonstrated. However, it has not previously been applied to the in-situ structural development investigation for the non-woven nanofiber mat stretching because of the aforementioned structural defects and complicated orientation development process.

The present paper deals with structural development of electrospun PVA non-woven nanofiber mat during uniaxial stretching. The macroscopic fiber orientation was evaluated by scanning electron microscopy (SEM) observation and in-situ stress-strain SAXS measurement. The macroscopic fiber orientation distribution was quantified by air void scattering in the vicinity of the beam center. Crystallite and molecular chain orientation were interpreted based on in-situ stress-strain WAXD measurement and polarized Fourier transform infrared spectroscopy (FT-IR) measurement, respectively.

2. Experimental

2.1. Fiber preparation

PVA (PVA217, degree of polymerization: 1700, degree of hydrolysis: 87.0–89.0%, manufactured by Kuraray Co., Ltd.) was dissolved in a water/*N*,*N*-dimethylformamide (DMF, Kishida Chemicals, 99.5%) (70/30, wt/wt) mixed solvent at 8.0 wt% concentration by stirring at 353 K. Water was purified with a Nano Pure Water system (Millipore, Billerica). Electrospun non-woven fiber mats were fabricated using a drum collector rotating at 50 rpm with a NANON-01A (MECC Co., Ltd.) nanofiber electrospinning device operating below 30% humidity. Diameter and width of the drum were 200 mm and 300 mm, respectively. The drum collector was used to fabricate large area non-woven mats with homogeneous surface characteristics. Significant nanofiber orientation was not observed on the non-woven nanofiber mats. The collector surface was covered with Al-foil to easily remove the nanofibers. The polymer solution was loaded into a plastic syringe and discharged from the nozzle (0.41 mm) at feed rate of 1.0 mL/h with applied voltage of 20 kV. The nozzle to collector distance was fixed at 150 mm. The fabricated non-woven nanofiber mats were dried under vacuum.

2.2. SEM observation

The non-woven nanofiber mat was held at both ends of the paper filters, and manually extended slowly. The elongated non-woven nanofiber mat was fixed on aluminum plates with double-faced tape. SEM observation was carried out using Real Surface View VE7800 (Keyence Co., Ltd.) with applied voltage of 1–10 kV. Samples were coated with an osmium layer (~3 nm) using HPC-1SW Hollow Cathode Plasma CVD (Shinkuu Device Co., Ltd.).

2.3. In-situ simultaneous SAXS and WAXD measurement during the tensile testing

In-situ simultaneous SAXS and WAXD measurements during the tensile testing were carried out at the BL03XU and BL40B2 beam line of SPring-8 (Japan Synchrotron Radiation Research Institute, Hyogo, Japan) using an X-ray source with wavelength, λ, of 0.1 nm. The scattering intensity was detected by a 3000 x 3000 pixel imaging plate for SAXS measurements, and a 1032 $\times$ 1032 pixel flat panel for WAXD measurements. The imaging plate and flat panel detectors were positioned 2230 mm and 71 mm from the sample, respectively. The scattering vector, $q = (4\pi/\lambda)\sin\theta$, where θ is the scattering angle, was calibrated by the peak positions of silver behenate for SAXS and cerium dioxide for WAXD measurements. The non-woven nanofiber mat was clamped at both ends with a tensile tester (Sentech Co., Ltd.), which was installed on the sample stage. The fixture allows a non-woven nanofiber mat to be stretched symmetrically in the lateral direction, which ensures that the X-ray beam always irradiates the same position during stretching. The sample dimensions were 30 mm length by 10 mm width, with 20 mm between clamps prior to deformation. Thickness of the sample was 160 μm. The non-woven nanofiber mat was symmetrically deformed stepwise to 10, 20, 30, 50, 100, 150% elongation at room temperature. The humidity was fixed at 55%. The stretching rate was set at 10 mm/min (50% strain/min). Measurements were made at each elongation step to obtain simultaneous SAXS and WAXD patterns. The sample was dried in a desiccator prior to testing, and the amount of adsorbed water was determined by thermal gravimetry analysis to be 5-8 wt%. The stretching speed, humidity and amount of adsorbed water were carefully controlled, to minimize their influence on orientation development.

2.4. Polarized FT-IR measurement

The deformed non-woven nanofiber mat was prepared by the same procedure described for SEM observation. Polarized FT-IR measurement was carried out at the BL43IR beam line of SPring-8 with a microscope system equipped with mercury-cadmium telluride detector operating in transmission mode. The aperture size was about 100 μm $\times$ 100 μm. A synchrotron radiation IR light source was used because of its high brilliance and wide wavenumber range from the visible to far IR regions [26]. The spectra were recorded from 800 to 4000 cm^{-1} with 4 cm^{-1} resolution.

3. Results and discussion

3.1. PVA nanofiber preparation

The quality of nanofibers fabricated by the electrospinning method is strongly influenced by the physical properties of the solvent, such as boiling point, volatility, viscosity, and surface tension. We found out that the water/DMF (70/30, wt/wt) solution allows stable PVA nanofiber fabrication for long period. The diameter of the nanofibers can be varied from about 190 nm to 1.5 μm by varying PVA concentration from 6.0 wt% to 16.0 wt%. Below 6.0 wt.% and above 16.0 wt.%, it is challenging to form high quality PVA nanofibers due to either extensive bead formation or solidification at the edge of syringe nozzle, respectively. At PVA concentration of 8.0 wt.% in water/DMF (70/30, wt/wt), an ideal Taylor cone structure was observed at feed rate of 1.0 mL/h with

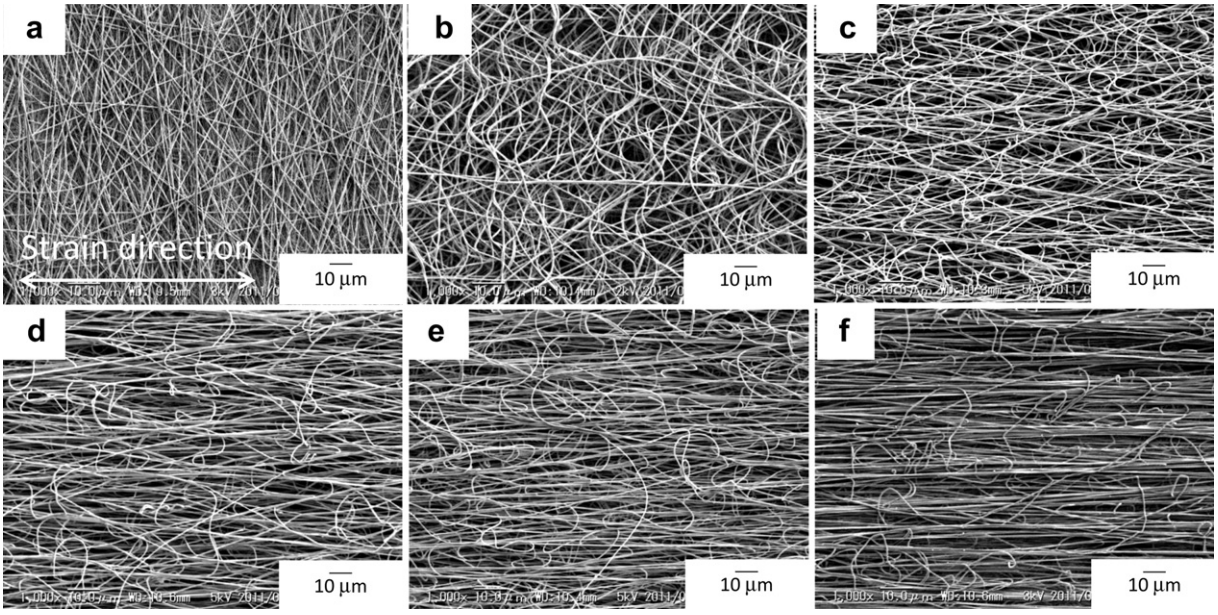

Fig. 1. SEM images of electrospun PVA non-woven nanofiber mat; (a) 0%, (b) 10%, (c) 30%, (d) 50%, (e) 100% and (f) 150% elongation.

applied voltage of 20 kV [27]. SEM observation revealed that the non-woven nanofiber mat was composed of randomly oriented PVA nanofibers with an average diameter of 360 nm and standard deviation of 36.3 nm (Fig. 1(a)).

3.2. Nanofiber orientation

The non-woven nanofiber mat was uniaxially deformed stepwise to 10, 20, 30, 50, 100, 150% elongation. The macroscopic nanofiber orientation was confirmed by SEM observation (Fig. 1). The as-spun non-woven nanofiber mat appears to be completely random. As deformation is applied, the nanofibers orient along the stretching direction. The average fiber diameter gradually reduces with elongation from 360 nm at initial to 300 nm at 150% elongation. These findings indicate that the nanofibers are simultaneously oriented and stretched in the tensile deformation. In the case of pure nanofiber orientation under deformation, there will be no change in fiber diameter.

In order to quantify the development of nanofiber orientation, stress-strain/SAXS measurements were performed at the BL40B2 beam line of SPring-8. The SAXS measurement was carried out at each elongation step. Fig. 2 shows the stress-strain curve on the experiment. Fig. 3 shows the 2-D SAXS patterns of the elongated PVA non-woven nanofiber mat at each elongation step. Scattering in the vicinity of the beam center is a result of the difference in electron density between the nanofibers and air voids, although some X-ray reflection from the edge of nanofibers may also be present. The scattering resulting from differences in the fibril structure and lamellar structure in the nanofibers can be ignored because the electron density difference of the structures is much smaller than that of the nanofibers and air voids. The isotropic scattering is confirmed by the SAXS pattern of the as-spun non-woven nanofiber mat (Fig. 3(a)). As the sample is deformed, the homogeneous intensity distribution becomes strongly anisotropic. Ruland's method was applied for the analysis of the streaks around the beam center [28,29]. This method is often used for the investigation of shish structure [30–32]. In this study, the angular spread (B_{obs}) of each azimuthal profile was determined as a function of the scattering vector, q. From the angular spread, the fibril length, l_f, and misorientation width, B_ϕ, were obtained from the following equation:

$$B_{obs}q = \frac{2\pi}{l_f} + B_\phi q \quad (1)$$

where B_{obs} is the full width at half maximum (FWHM) of the azimuthal profile from the equatorial streak fitted with a Lorentz function. The misorientation width was obtained from the slope of the $B_{obs}q$ vs. q plot. The value of B_ϕ represents the orientation distribution of longitudinal voids in the non-woven nanofiber mat. Therefore, narrow misorientation width represents a high degree of nanofiber orientation. Fig. 4 shows development of the misorientation width with elongation. The misorientation width rapidly decreases at the beginning of stretching, which is attributed to the macroscopic orientation of the nanofibers along the stretching direction. Above 50% elongation, the misorientation width approaches a saturation value. The misorientation width of at 100% elongation (19.7), is almost same as that of at 150% elongation

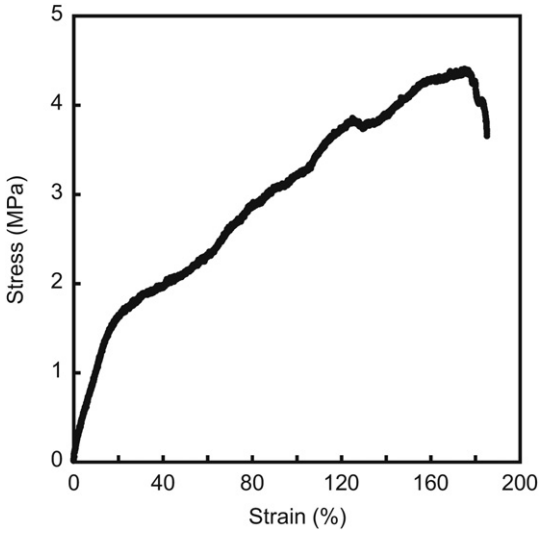

Fig. 2. Stress-strain curve for electrospun PVA non-woven nanofiber mat obtained by the homemade tensile testing device deformed at rate of 10 mm/min.

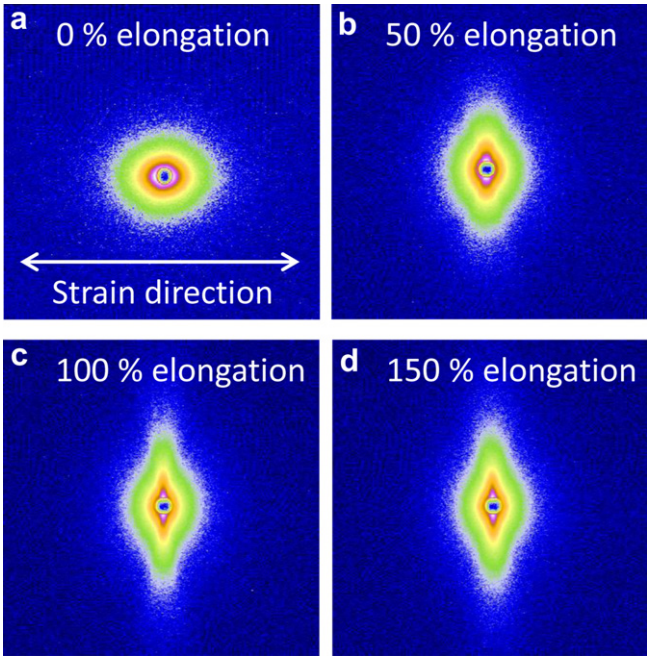

Fig. 3. 2-D SAXS patterns of elongated electrospun PVA non-woven nanofiber mat; (a) 0%, (b) 50%, (c) 100% and (d) 150% elongation.

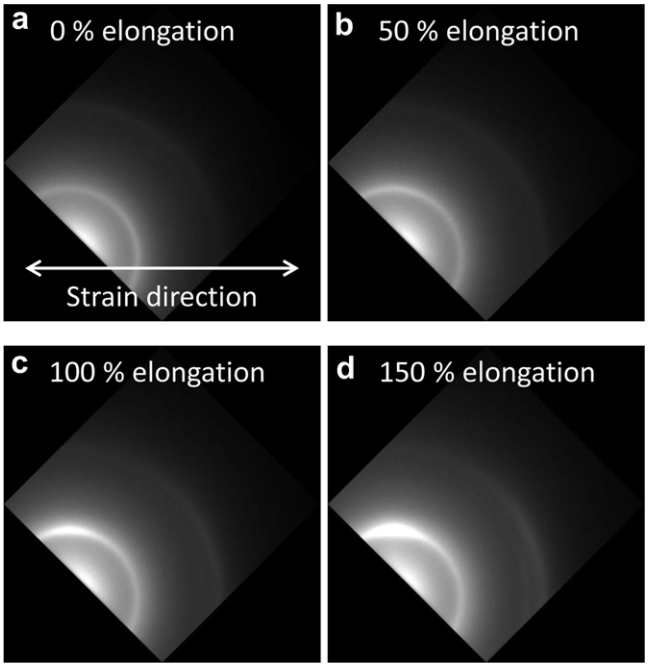

Fig. 5. 2-D WAXD patterns of elongated electrospun PVA non-woven nanofiber mat collected under uniaxial deformation; (a) 0%, (b) 50%, (c) 100% and (d) 150% elongation.

(19.4). Therefore, the macroscopic nanofiber orientation levels off above 50% elongation.

3.3. Crystallite orientation

Typical 2-D WAXD patterns obtained simultaneously on the uniaxial stretching are shown in Fig. 5. The as-spun non-woven nanofiber mat exhibits a circular 2-D diffraction pattern with homogeneous intensity distribution. The strongest intensity diffraction at $q = 13.8\ \mathrm{nm}^{-1}$ is identified as the (101) and $(10\bar{1})$ diffraction of PVA crystallites [33]. The diffraction intensity is found to converge on the equator with increasing strain, which suggests that the (101) and $(10\bar{1})$ lattice planes rotate along the equator with increasing strain. The intensity distribution of the (101) and $(10\bar{1})$ reflection on the azimuthal WAXD profile were used to quantify crystallite orientation. Herman's orientation function (f) is given by the following equation:

$$f = \frac{1}{2}\left(3 < \cos^2\phi > - 1\right) \tag{2}$$

where, ϕ is the angle between the polymer chain axis and the (101) and $(10\bar{1})$ lattice planes. A square averaged cosine of ϕ is defined by

$$\left\langle \cos^2\phi \right\rangle = \cos^2\theta \left\langle \cos^2\beta \right\rangle = \frac{\cos^2\theta \int_0^{\pi/2} I(\beta)\sin\beta\cos^2\beta \mathrm{d}\beta}{\int_0^{\pi/2} I(\beta)\sin\beta \mathrm{d}\beta} \tag{3}$$

where $I(\phi)$ is the 1-D intensity profile along with the azimuthal angle, β is the azimuthal angle, and θ is scattering angle. The value of f is 1 and −0.5 when the polymer chains are aligned either perfectly parallel or perpendicular to the fiber axis, respectively. When f is zero, there is random orientation. The simplified method for the calculation of orientation function was applied in this case. The f value is calculated from the equation

$$f = \frac{180 - \mathrm{FWHM}}{180} \tag{4}$$

where f is the orientation factor of the crystallites. The azimuthal profiles of the (101) and $(10\bar{1})$ peaks were calculated through peak fitting with a Lorentz to determine FWHM [15].

The relationship between the orientation factor and elongation is shown in Fig. 6. The orientation factor is almost zero for the as-spun non-woven nanofiber mat, which is consistent with SEM and SAXS measurements discussed earlier and confirms that there is no initial orientation in the sample. Below 50% elongation, the rapid increase in orientation factor can be attributed to two different mechanisms: macroscopic nanofiber orientation, and microscopic orientation of the crystallites and molecular chains. Within each filament, the crystallites and molecular chains should

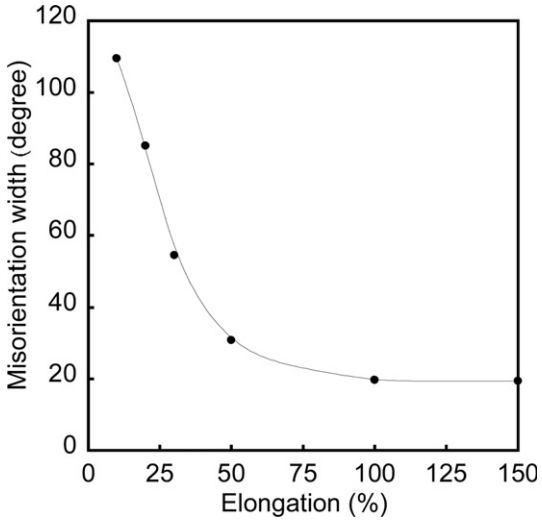

Fig. 4. Variation of the misorientation width as a function of elongation.

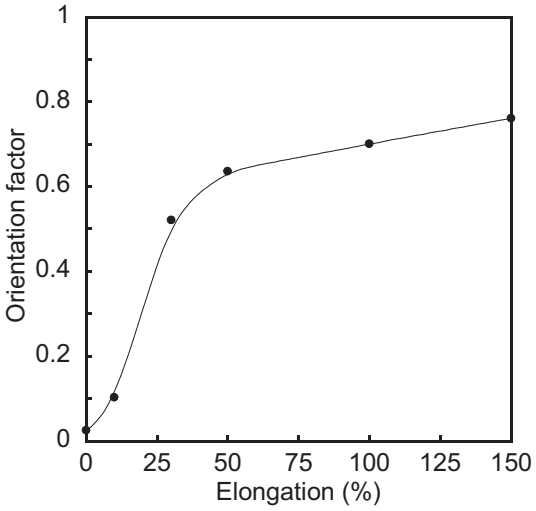

Fig. 6. Variation of orientation factor estimated from the 2-D WAXD patterns as a function of elongation.

initially be oriented in the fiber axial direction due to the combination of shearing forces when the polymer solution flows through the capillary needle, and Coulombic forces when the jet is elongated by the applied electric field during the electrospinning process [14–17]. The shear force and Coulombic force promote microscopic orientation of the crystallites and molecular chains within the fibril, which are then fixed due to the combination of confinement within the small diameter of the nanofiber, and rapid solvent evaporation. Therefore, the orientation of the nanofibers at the initial stage of stretching should be responsible for the rapid increase in orientation factor. However, the continuous increase in orientation factor above 50% elongation is in contrast with the plateau observed with the misorientation width in Fig. 4. This indicates that the microscopic crystallite orientation continues to develop as the nanofiber is stretched, which is independent from the macroscopic nanofiber orientation.

The polarized FT-IR spectra of the as-spun and the elongated non-woven nanofiber mat are shown in Fig. 7. The solid and dotted lines correspond to polarized FT-IR spectra of the parallel and perpendicular electric vector of the incident IR beam with respect to the stretching direction, respectively. The dashed line is the

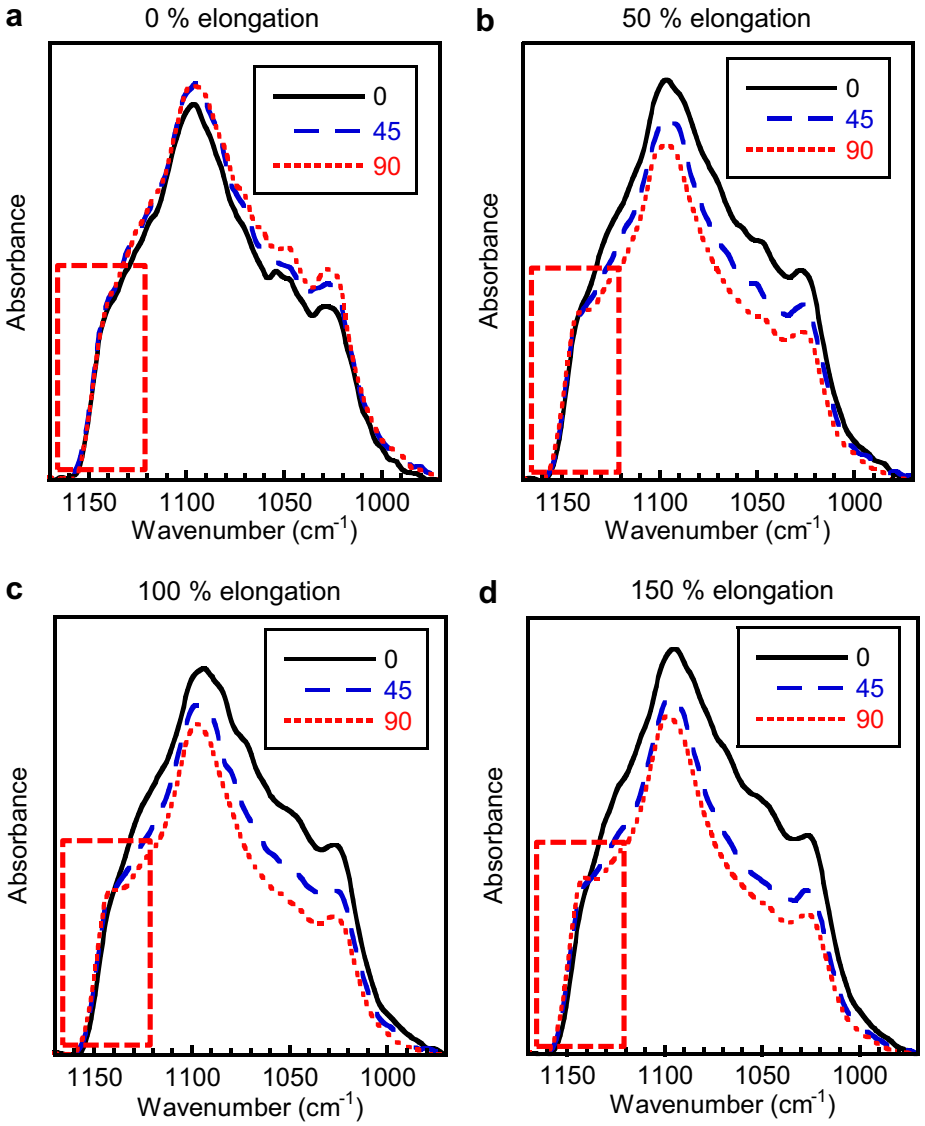

Fig. 7. Polarized FT-IR spectra of elongated electrospun PVA non-woven nanofiber mat; (a) 0%, (b) 50%, (c) 100% and (d) 150% elongation.

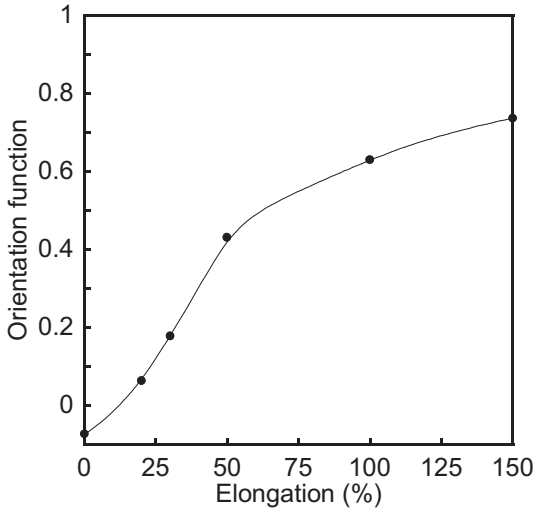

Fig. 8. Variation of orientation function estimated from the polarized FT-IR spectra as a function of elongation.

polarized FT-IR spectra measured with electric vector of the incident IR beam oriented 45-degrees from the stretching direction. The absorbance band at 1141 cm^{-1} is sensitive to crystallization [34–38], and shows differences in absorbance between the parallel and perpendicular polarized IR measurements for the elongated non-woven nanofiber mat. This crystallization-sensitive band is useful to determine crystallite orientation because there is a perpendicular transition moment against the polymer chain axis, which results in strong dichroism [37,38]. In order to quantify the degree of molecular chain orientation, the dichroic ratio, D, and Herman's orientation function, f, were evaluated by the following expressions:

$$D = \frac{A_0}{A_{90}} \tag{5}$$

$$f = \frac{2}{3\cos^2\alpha - 1}\frac{D-1}{D+2} \tag{6}$$

where A_0 and A_{90} are the parallel and perpendicular polarized IR absorbance intensities of the crystallization-sensitive band, respectively, and α is the angle between the chain axis and the transition dipole moment of a particular vibration mode. The orientation function calculated from the dichroic ratio represents the degree of the molecular chain orientation. For a randomly oriented sample, f is equal to 0, and for a perfectly uniaxially oriented sample, where all molecular chains orient along the fiber axis, f is equal to 1. Fig. 8 shows the evolution of the orientation function as a function of nanofiber mat elongation. The orientation function rapidly increases up to 50% elongation, similar to the WAXD results, which suggests that the b-axis direction of the PVA crystallites is oriented in the stretching direction. As elongation is increased further, the orientation function continues to increase. This indicates that the microscopic molecular chain orientation consisting of both crystallite regions and amorphous chains develops by the nanofiber stretching after saturation of the macroscopic nanofiber orientation.

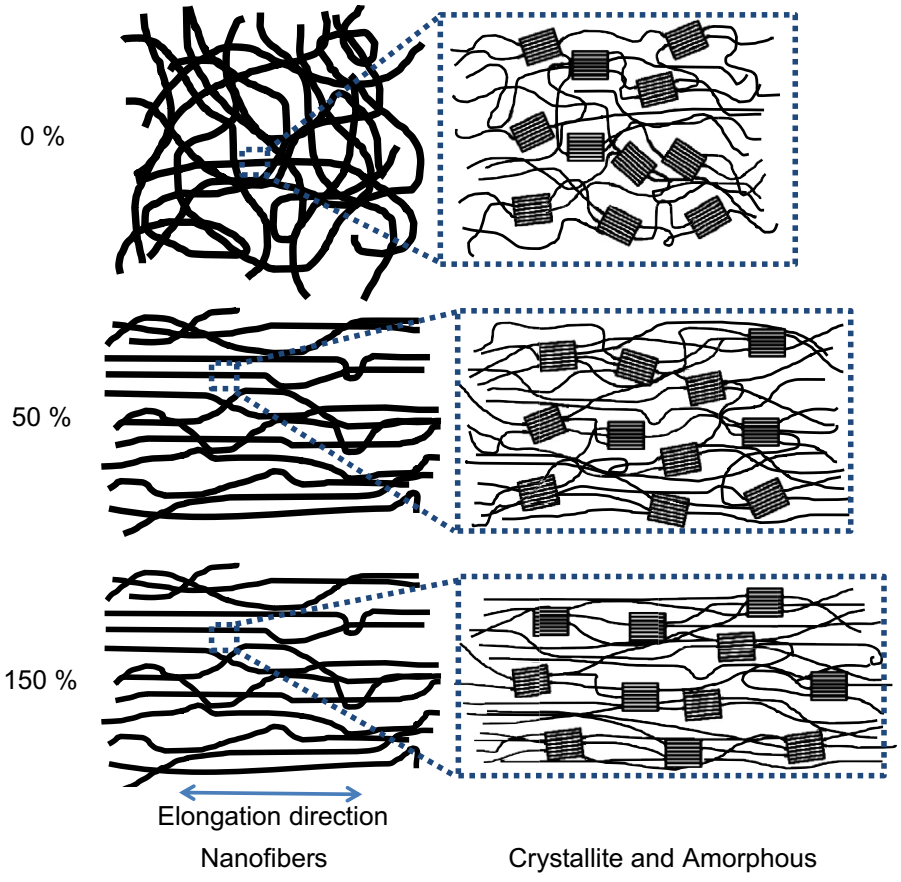

Fig. 9. Schematic representation of macroscopic and microscopic structural development during uniaxial stretching of PVA non-woven nanofiber mats.

Stress-induced crystallization is a potential mechanism that may occur during uniaxial stretching deformation. In the case of PVA, IR absorption at the crystallization-sensitive region around 1141 cm^{-1} increases linearly with degree of crystallinity [34,35]. In Fig. 7, the crystallization-sensitive band intensity of the nanofiber mat is constant throughout the stretching. Furthermore, there is no evidence of stress hardening from the stress-strain curve of the non-woven nanofiber mats. These results indicate that stress-induced crystallization is negligible during the uniaxial deformation of PVA non-woven nanofiber mats.

4. Conclusion

We have presented the structural development of electrospun non-woven PVA nanofiber mats during uniaxial stretching. The development of structure was discussed in terms of macroscopic nanofiber orientation and microscopic crystallite and molecular chain orientation. Our proposed structural model for the uniaxial stretching of the nanofiber mat consists of macroscopic orientation of the initial isotropic nanofiber mat that saturates on the way of stretching, and a continuous microscopic orientation that persists up to higher deformation. This mechanism of orientation is shown schematically in Fig. 9. This is the first report on the in-situ analysis of the uniaxial stretching of an electrospun nanofiber mat, and we have considered nanofiber orientation and the crystallite and molecular chain orientation. We anticipate that this knowledge will contribute to material design of non-woven nanofiber materials for industrial applications.

Acknowledgments

The present work is supported by a Grant-in-Aid for the Global COE Program, “Science for Future Molecular Systems” and a Grant-in-Aid for Scientific Research on Innovative Area (20106002) from the MEXT. The synchrotron radiation experiments were performed at the BL03XU(2011A7232), BL40B2 (2011A1001) and BL43IR (2010B1344, 2011B1320) in the SPring-8 with the approval of the Japan Synchrotron Radiation Research Institute (JASRI).

References

[1] Arinstein A, Burman M, Gendelman O, Zussman E. Nat Nanotechnol 2007;2:59–62.
[2] Ji Y, Li B, Ge S, Sokolov JC, Rafailovich MH. Langmuir 2006;22:1321–8.
[3] Zusssman E, Yarin AL, Bazilevsky AV, Avrahami R, Feldman M. Adv Mater 2006;18:348–53.
[4] Ding Z, Salim A, Ziaie B. Langmuir 2009;25:9648–52.
[5] Baumgarten PK. J Colloid Interface Sci 1971;36:71–9.
[6] Doshi J, Reneker DH. J Electrostatics 1995;35:151–60.
[7] Takahara A, Hadano M, Yamaguchi T, Otsuka H, Kidoaki S, Matsuda T. Macromol Symp 2005;224:207–18.
[8] Yano T, Yah WO, Yamaguchi H, Terayama Y, Nishihara M, Kobayashi M, et al. Chem Lett 2010;39:1110–1.
[9] Yano T, Yah WO, Yamaguchi H, Terayama Y, Nishihara M, Kobayashi M, et al. Polym J 2011;43:838–48.
[10] Qian YF, Su Y, Li XQ, Wang HS, He CL. Iran Polym J 2010;19:123–9.
[11] Han SO, Son WK, Youk JH, Lee TS, Park WH. Mater Lett 2005;59:2998–3001.
[12] Megelski S, Stephens JS, Chase DB, Rabolt JF. Macromolecules 2002;35:8456–66.
[13] Kongkhlang T, Kotaki M, Kousaka Y, Umemura T, Nakaya D, Chirachanchai S. Macromolecules 2008;41:4746–52.
[14] Yoshioka T, Dersch R, Tsuji M, Schaper AK. Polymer 2010;51:2383–9.
[15] Kongkhlang T, Tashiro K, Kotaki M, Chirachanchai S. J Am Chem Soc 2008;130:15460–6.
[16] Kakade MV, Givens S, Gardner K, Lee KH, Chase DB, Rabolt JF. J Am Chem Soc 2007;129:2777–82.
[17] Rungswang W, Kotaki M, Shimojima T, Kimura G, Sakurai S, Chirachanchai S. Macromolecules 2011;44:9276–85.
[18] Lee K, Lee B, Kim C, Kim H, Kim K, Nah C. Macromol Res 2005;13:441–5.
[19] Dupaix RB, Hosmer JED. Int J Struct Changes Solids 2010;2:9–17.
[20] Masunaga H, Sasaki S, Tashiro K, Hanesaka M, Takata M, Inoue K, et al. Polym J 2007;39:1281–9.
[21] Miyazaki T, Hoshiko A, Akasaka M, Shintani T, Sakurai S. Macromolecules 2006;39:2921–9.
[22] Miyazaki T, Hoshiko A, Akasaka M, Sakai M, Takeda Y, Sakurai S. Macromolecules 2007;40:8277–84.
[23] Kojio K, Matsuo K, Motokucho S, Yoshinaga K, Shimodaira Y, Kimura K. Polym J 2011;43:692–9.
[24] Li X, Mao Y, Ma H, Zuo F, Hsiao BS, Chu B. Polymer 2011;52:4610–8.
[25] Kawakami D, Ran S, Burger C, Orta CA, Sics I, Chu B, et al. Macromolecules 2006;39:2909–20.
[26] Shinoda K, Yamakata M, Nanba T, Kimura H, Moriwaki T, Kondo Y, et al. Phys Chem Minerals 2002;29:396–402.
[27] Larrondo L, Manley RSJ. J Polm Sci Part B 1981;19:909–20.
[28] Ruland W. J Polym Sci Part C 1969;28:143–51.
[29] Ruland W. J Appl Phys 1967;38:3585–9.
[30] Somani RH, Yang L, Hsiao BS, Sun T, Pogodina NV, Lustiger A. Macromolecules 2005;38:1244–55.
[31] Patil N, Balzano L, Portale G, Rastogi S. Macromolecules 2010;43:6749–59.
[32] Keum JK, Zuo F, Hsiao BS. Macromolecules 2008;41:4766–76.
[33] Bunn CW. Nature 1948;161:929–30.
[34] Tadokoro H, Seiki S, Nitta I. Bull Chem Soc Jpn 1955;28:559–64.
[35] Tadokoro H. Bull Chem Soc Jpn 1959;32:1334–9.
[36] Hibi S, Maeda M, Makino S, Nomura S, Kawai H. SEN-I GAKKAISHI 1971;27:246–53.
[37] Krimm S, Liang CY, Sutherland GBBM. J Polym Sci 1956;22:227–47.
[38] Tadokoro H, Seki S, Nitta I. J Polym Sci 1956;22:563–6.